Hindawi
Shock and Vibration
Volume 2017, Article ID 6209205, 17 pages
https://doi.org/10.1155/2017/6209205

Research Article

Experimental Study on Variation Rules of Damping with Influential Factors of Tuned Liquid Column Damper

Yang Yu,[1,2,3] Lixin Xu,[1,2] and Liang Zhang[4]

[1]*State Key Laboratory of Hydraulic Engineering Simulation and Safety, Tianjin University, Tianjin 300350, China*
[2]*Collaborative Innovation Center for Advanced Ship and Deep-Sea Exploration, Shanghai 200240, China*
[3]*State Key Laboratory of Ocean Engineering, Shanghai Jiaotong University, Shanghai 200240, China*
[4]*Beijing Spacecrafts, Beijing 100094, China*

Correspondence should be addressed to Lixin Xu; lixin.xu@tju.edu.cn

Received 2 May 2017; Revised 16 August 2017; Accepted 26 September 2017; Published 26 October 2017

Academic Editor: Felice Ponzo

A tuned liquid column damper (TLCD) is a more effective form of passive control for structural vibration suppression and may be promising for floating platform applications. To achieve good damping effects for a TLCD under actual working conditions, factors that influence the damping characteristics need to be identified. In this study, the relationships between head loss coefficients and other factors such as the total length of the liquid column, opening ratio, Reynolds number, Kc number, and horizontal length of the liquid column were experimentally investigated. By using a hydraulic vibration table, a vibration test system with large-amplitude motion simulation, low-frequency performance, and large stroke force (displacement) control is devised with a simple operation and at low cost. Based on the experimental method of uniform design, a series of experimental studies were conducted to determine the quantitative relationships between the head loss coefficient and other factors. In addition, regression analyses indicated the importance of each factor affecting the head loss coefficient. A rapid design strategy of TLCD head loss coefficient is proposed. This strategy can help people conveniently and efficiently adjust the head loss coefficient to a specified value to effectively suppress vibration.

1. Introduction

The dynamic response of tall structures such as high-rise buildings and ocean platforms is highly apparent under external loads [1–3]. The vibration of such structures can be suppressed by strengthening the structure and increasing its size; however, this leads to a significant increase in its cost. To overcome this problem, in recent years, additional dampers have been widely applied to suppress vibrations. Dampers are used in high-rise buildings to reduce the impact of wind and earthquake loads and in offshore platforms, to reduce the effect of waves.

Thus far, few studies have focused on the motion suppression of floating platforms in complex operating environments. Structural vibration control methods can be categorized into three types: active, semiactive, and passive. Passive control is usually used to suppress the vibration of structures by dissipating and absorbing energy. Passive control dampers are of three main types: tuned mass damper (TMD), tuned liquid damper (TLD), and tuned liquid column damper (TLCD). Of these, a TLCD, which was developed based on the TLD, is the most effective.

The main body of the TLCD is a U-shaped water tunnel that consists of two vertical columns connected by a horizontal column filled with liquid, usually water. An orifice plate is installed at the center of the horizontal column; it changes the damping effect by adjusting the discharge passing through. When the main structure vibrates, a part of the energy is transferred to the liquid column, which absorbs the same energy through its movement. At the same time, the pressure difference between the two vertical liquid columns produces a damping force that suppresses the vibration of the main structure. Although few studies have investigated the application of TLCDs to floating platforms, many existing structures on such platforms, such as oil containers, fresh water containers, and even floating tanks, could be modified

to incorporate TLCDs. In addition, given that TLCDs have low manufacturing and installation costs as well as relatively low maintenance requirements, they might actually be greatly advantageous for applications to floating platforms.

Sakai et al. [4] first proposed TLCDs in 1989. Hochrainer [5] presented a detailed derivation of their working principle and applied a bang-bang control scheme based on linear optimal control to reduce transient vibrations. Hitchcock et al. [6–8] optimized the original TLCDs by varying their cross section to overcome their narrow frequency band. They also studied the damping effect of several TLCDs and its influence on the vibration frequency range and head loss coefficient. Lee et al. [9–11] built a structural model on a shaking table with acceleration control and experimentally implemented a TLCD to investigate the control of the response of building structures excited by earthquakes. By comparing the liquid column amplitude and energy consumption between a TLD and a TLCD with the same size and damping effect, they found that the natural vibration frequency of the TLCD has a greater influence on the liquid column amplitude, leading to higher energy consumption for the main structure. In addition, by integrating the characteristics of both TLD and TLCD, they designed a bidirectionally tuned liquid column and sloshing damper that suppressed vibrations along the two principal axes of a structure. Chaiviriyawong et al. [12] used a computational fluid dynamics model to study the variation of the flow velocity in the elbow between horizontal and vertical liquid columns of different widths. Chan and Ding [13] conducted structural experiments to compare the damping effects of TLCDs with liquid columns of different lengths and tilt angles. To make TLCDs more effective in reducing structural vibrations, Al-Saif et al. [14] modified a TLCD by placing a coated steel ball as a moving orifice inside the horizontal section of the damper instead of the orifice plate and disturbed the flow so as to improve the absorber's attenuation performance. In recent years, TLCDs of different forms have been developed as their range of applications has broadened. Huo and Li [15] assessed the application of a TLCD to the control system of a jacket platform and analyzed the control performance of a circular TLCD on suppressing the coupled torsion vibration of an offshore platform under waves and earthquake loads. Lee et al. [16, 17] were the first to apply a TLCD in a floating platform and provide experimental verification. Moreover, they compared the effects of two different installation arrangements: on the floating platform and underwater.

For the TLCD to have good damping effects, the functional relationships that determine the damping characteristics must be identified. The most direct way to do so is to adjust the relevant parameters of the orifice plate. For a given size and conditions such as external excitation frequency and quality, Chen and Chao [18] proposed a method for calculating the optimal damping ratio for a TLCD that has the optimum damping effect on the main structure. Additionally, the influence of the optimal damping ratio on the harmonic response was discussed for different effective length ratios. Shum and Xu [19, 20] developed a closed-form optimal solution scheme for a TLCD-structure system and determined its optimal damping ratio for suppressing harmonic vibrations. Chakraborty et al. [21] discussed the optimization of the damping coefficient and other parameters with a reasonable maximum amplitude of liquid oscillation. Yalla and Kareem [22] varied the inclination angle of the orifice plate to determine the optimal damping ratio for an orifice plate with a narrow slit and confirmed that the damping ratio of the TLCD strongly influences the amplitude of oscillations in the main structure. Lee et al. [11] discussed the correlation between the liquid motion amplitude and different external excitation amplitudes under different frequency ratios and damping coefficients and analyzed the relationships between the excitation amplitude and the parameters related to the TLCD. Furthermore, some researchers performed experimental tests. Wu et al. [23–26] proposed an analytical method for determining the optimal damping ratio with variable cross sections and found that it is inversely proportional to the external excitation amplitude. According to the two-degree-of-freedom (2-DOF) motion equation and transfer relationship between the main structure and the TLCD, they established an experimental measurement method for the head loss coefficient based on the equivalent linear damping item and motion amplitude. The head loss for a TLCD is mainly produced by oscillation flow in the U-shaped tube. When oscillation occurred along the direction of tube flow, considering the Reynolds number, Kc number, and relative roughness of the cylinder surface, Sarpkaya and Isaacson [27–30] plotted the variation in the curves of the drag coefficient C_D and inertial force coefficient C_M for the oscillation flow of a circular cylinder after numerous experiments under different conditions. They also performed extensive analyses based on changes in the cylinder force and energy transmission. Carberry [31] compared and summarized the advantages and disadvantages of existing forced oscillation tests. They investigated the effect of the Reynolds number on the results of the experimental test when the oscillation is perpendicular to the direction of tube flow. Morse and Williamson [32] confirmed that the fluid force of self-excited vibrations is similar to that of forced oscillation under conditions in which the amplitude, frequency, and Reynolds number are equal. Note that these damping characteristic experiments are only applicable to a cylinder. The damping characteristics differ for orifice plates having a shape other than a circle or square. A similar problem is the vortex-induced vibration in marine engineering [33, 34]. Thus far, few studies have focused on the orifice plate characteristics and optimization damping ratio of TLCDs. In addition, the nonlinear damping term is usually simplified to be linear. Hence, several issues could be studied further: the functional relationship between the head loss coefficient and the orifice plate properties; the degree to which the opening rate and other TLCD parameters affect head loss; and guidelines for quickly adjusting the head loss coefficient to the specified value during engineering practice.

Experimental studies on the damping characteristics of a TLCD can be performed using an offshore engineering model basin or a vibration test system on land. The high construction cost of the former makes it impossible to repeat experiments. In addition, such devices cannot directly control the size of the external force applied to the measured model, and the wave force acting on the structure can only be

indirectly changed by adjusting the wave height and period. Thus, measuring the head loss coefficient of a TLCD on a floating platform model is extremely difficult. An on-land vibration test system is a good alternative because of its low cost and easy control. On the other hand, such systems are always designed for civil structures or machines, which differ from floating platforms in some respects such as natural vibration period, amplitude, and external environment. Because existing onshore test systems cannot effectively and inexpensively simulate the working conditions on a floating platform, it is desirable to design an alternative device with large stroke force control components for simulating large-amplitude motions at low frequency.

Current onshore vibration test systems mainly include electromagnetic vibration and electrohydraulic servo test systems. An electromagnetic vibration test system, which is costly and shows low total harmonic distortion (THD), is mainly used for high-frequency (tens to thousands of Hertz) simulation. Kim et al. [35] optimized the dynamic performance of electromagnetic exciters by using finite element analysis. By using a numerical simulation to design the control scheme for an electromagnetic actuator with a 10 kN load, Li et al. [36] found that high-precision control of the actuator signal could be achieved by adaptive inverse control theory. Zhu et al. [37] designed a new type of micro electromagnetic vibration exciter whose resonance frequency could be controlled without changing the total damping. Oliver and Priya's [38] four-bar magnet geometry increased the output power of the electromagnetic vibration exciter and the accuracy of predicting the optimal load resistance.

The other major type of onshore system is an electrohydraulic servo test system, which produces various types of oscillatory waves through a dynamic loading device and simulates the vibration for an experimental subject on a rigid surface. Despite its speed and high power, its precision is slightly less than that of the electromagnetic vibration test system. Moreover, its running and maintenance costs are quite high. Conte and Trombetti [39] found a potentially strong dynamic interaction between the oil column in the actuator and the payload when their frequencies were similar in a uniaxial servohydraulic shaking table system. Stehman and Nakata [40] used force feedback to ensure stable motion of the shaking table in a perfectly balanced position to optimize acceleration control. Jianjun et al. [41] discussed the use of the least mean square (LMS) adaptive filtering algorithm to control the amplitude and phase of the acceleration signal so as to suppress higher harmonics and reduce distortion [41]. To eliminate adverse effects on the acceleration of vibration control, Dozono et al. [42] introduced adaptive filtering compensation (AFC) to the control theory of shaking tables. To reduce the maintenance and operation cost, Ye et al. [43] invented a pneumatic shaking table that used compressed air instead of electricity as the transmission medium and changed the loading mode from hydraulic to pneumatic actuation. This type of shaking table provides more stable low-frequency harmonic frequencies (above 3 Hz).

An investigation of a shaking table test system reveals that an electromagnetic vibration system is usually used to study the strength and elastoplastic properties of the sample. Conducting experiments with large displacements is difficult because the maximum amplitude of the electromagnetic vibration system is only 5–35 mm. However, electrohydraulic servo test systems suffer from some drawbacks. The input signal is always the acceleration or displacement, which is seldom loaded directly. Nonlinear factors such as the delay of the servo valve actuator, compression of liquid in the actuator, and closeness of the actuator greatly influence precision, especially for a small electric hydraulic servo vibration system. The distortion of the response curve is a serious impediment to processing experimental data at low frequencies (0.2–1 Hz) because the high-order harmonic generation cannot be eliminated. In this study, the frequency of the shaking table must be 0.5–1.5 Hz to simulate the horizontal movement accurately. Moreover, the maximum displacement amplitude is set above 100 mm to simulate the resonance phenomenon between the shaking table and the TLCD. Hence, conducting experiments with an electrohydraulic servo test system is extremely difficult.

As discussed above, it is challenging to find an available test system simultaneously equipped with large-amplitude motion simulation, low-frequency performance, and large stroke force control. In this study, a vibration test system that satisfies the above requirements is independently designed to achieve harmonic wave force loading based on a small hydraulic shaking table with a custom-made loading system and a device for changing stiffness. In the low-frequency range of 0.5–1.5 Hz, the maximum displacement amplitude is above 100 mm without any high-order harmonic generated during the loading process. The THD is less than 0.5%. According to the experimental data, the head loss coefficient of the nonlinear damping term of the TLCD is calculated based on the energy transmission between the TLCD and the experimental vibration system. The functional relationship between the head loss coefficient and the orifice plate properties or the TLCD's relevant parameters is also investigated. This paper is divided into two parts: the first part describes the rationale for independently designing an available test system with large-amplitude motion simulation, low-frequency performance, and large stroke force control, and the second part discusses the application of a uniform design to determine the functional relationship between the head loss coefficient and the natural frequency of the TLCD, orifice plate parameters, Reynolds number or Kc number in the liquid column of the TLCD, or ratio of the horizontal column to the vertical column. Finally, a type of rapid design strategy is proposed for the TLCD head loss coefficient under working conditions.

2. Design of Experimental System

As noted earlier, a TLCD, a type of passive vibration control device, is widely used in structures such as high-rise buildings. A TLCD suppresses motion in a structure by transferring part of the kinetic energy from the main structure to the liquid column, which causes the latter to undergo severe sloshing and absorb energy. In addition, part of the energy is consumed by damping effects in the TLCD. As shown in Figure 1, L_d is the total length of the liquid column,

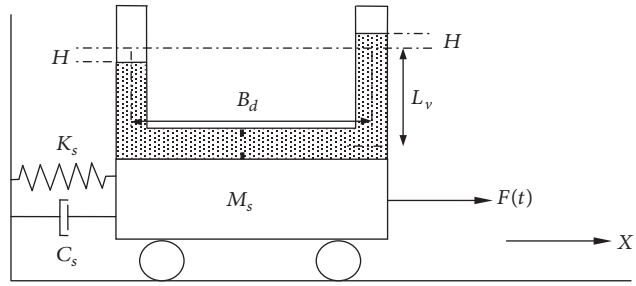

Figure 1: Schematic diagram of TLCD.

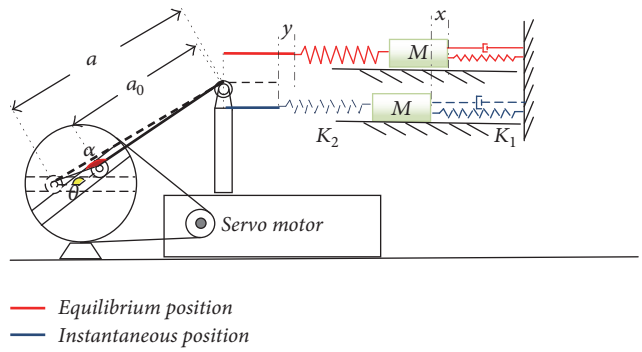

Figure 2: Schematic diagram of vibration test system with large motion amplitude and force control.

which can be expressed as $L_d = B_d + 2L_v$; vertical columns length is denoted by L_v; horizontal column length is denoted by B_d; and head loss coefficient is denoted by h_d. By using the Lagrange equation and energy method, the 2-DOF motion equations of the TLCD fluid column and the main structure are established as follows:

$$\begin{aligned} &M_s\ddot{X} + C_s\dot{X} + K_sX = F(t) - \rho_d A_d B_d \ddot{H} - \rho_d A_d L_d \ddot{X} \\ &\rho_d A_d L_d \ddot{H} + \frac{1}{2}\rho_d h_d A_d \left|\dot{H}\right| \dot{H} + 2\rho_d g A H \\ &\quad = -\rho_d B_d A_d \ddot{X}. \end{aligned} \tag{1}$$

Equations (1) show that experimental studies on the TLCD need a force control vibration test system. In addition, for the onshore simulation of a floating platform with the vibration characteristics of the above TLCD, the vibration test system should be capable of large-amplitude motion simulation, low-frequency performance, and large stroke force control. As mentioned earlier, because it is difficult to find a test system that satisfies these requirements, the system is independently designed in this study. Its working principle and design scheme are illustrated in Figure 2.

Figure 2 shows the operational principle of the loading device. Here, K_1 is the equivalent stiffness of the required measured object; K_2, the stiffness of the extension spring; M, the quality of the required loading object; E, the elastic modulus of the wire rope; A, the cross-sectional area of the wire rope; l_0, the length of the wire rope between the extension spring end and the belt pulley; a_0, the length of the wire rope from the fixed pulley to the slider before starting the device; a, the length of the wire rope from the fixed pulley to the slider at a given time after starting the device; r, the radius of the belt wheel; θ, the instantaneous rotation angle of the belt wheel; α, the angle corresponding to a in a triangle constituted by a, a_0 and the line connecting these two endpoints; x, the displacement of the object under instantaneous rotation; y, the displacement between the extension spring and the fixed pulley under instantaneous rotation; and ω, the rotational frequency of the belt pulley, usually $a_0 > 10r$. After starting the motor, the object moves from the equilibrium position to the instantaneous position. At the same time, the length variation of the wire rope is $a - a_0 - y$. In the triangle constituted by a, a_0 and the line connecting these two endpoints, Taylor expansion is used on the expression for a obtained by the cosine theorem. When $a_0 > 10r$, the higher-order terms are infinitesimal. Keeping the first-order term of the Taylor expansion of a gives

$$a = a_0 + \frac{r^2 + ra_0}{a_0} - \frac{r^2 + ra_0}{a_0}\cos\omega t. \tag{2}$$

When the wire rope is tensed at the equilibrium position, the prestressed forces from the extension spring and the measured object are equal and opposite in sign. The measured object is subjected to the force produced by the deformation quantity of the extension spring at the time of belt pulley turning. The equation of motion for object M can be

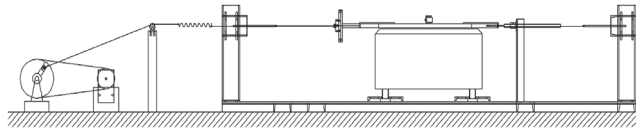

Figure 3: Design drawing of experimental installations.

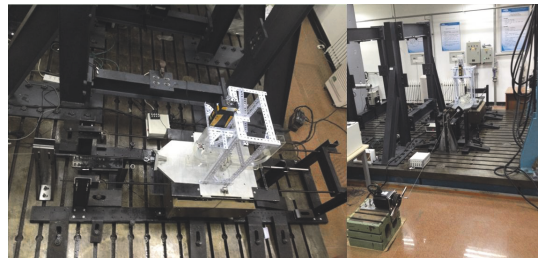

Figure 4: Photographs of experimental testing system.

expressed as $M\ddot{x} + Cx + K_1x = K_2(y - x)$. According to the force equilibrium between the extension spring and the wire rope, y is obtained as follows:

$$\frac{EA\left(a - a_0 - y\right)}{l_0} = K_2\left(y - x\right)$$
$$y = \frac{EA\left(a - a_0\right) + K_2 l_0 x}{EA + K_2 l_0}. \tag{3}$$

At the moment of belt pulley turning, the external force acting on the object is obtained as follows:

$$F = K_2\left(y - x\right) = K_2\left(\frac{1}{1 + K_2/\left(EA/l_0\right)}\left(a - a_0\right) - \frac{1}{1 + K_2/\left(EA/l_0\right)}x\right). \tag{4}$$

Thus, the resulting motion equation forms are expressed as follows:

$$M\ddot{x} + C\dot{x} + Kx = F_0 + F_t\cos\omega t$$
$$K = K_1 + K_2\frac{EA}{EA + K_2 l_0}$$
$$F_0 = \frac{K_2 EA}{EA + K_2 l_0}\frac{r^2 + ra_0}{a_0} \tag{5}$$
$$F_t = \frac{K_2 EA}{EA + K_2 l_0}\frac{r^2 + ra_0}{a_0}.$$

The expression for z is given as

$$z = x - \frac{K_2 EA}{K_1 EA + K_1 K_2 l_0 + K_2 EA}\frac{r^2 + ra_0}{a_0}. \tag{6}$$

Equation (5) can then be simplified as

$$M\ddot{z} + C\dot{z} + Kz = F_t\cos\omega t. \tag{7}$$

Before starting the experiments, pretension should be imposed on the wire rope and extension spring to keep them tightening during the experiments. This test system also simulates the static and displacement loading conditions. When the angle of rotation of the belt pulley is fixed at $\omega t = \pi/2$, the constant external force acting on the object is expressed as

$$F_{\text{Constant}} = \frac{K_2 EA}{EA + K_2 l_0}\left(\frac{r^2 + ra_0}{a_0}\right). \tag{8}$$

By removing the tension adjusting spring, that is, using the displacement loading method alone, the displacement variation of the object is expressed as

$$x = \frac{r^2 + ra_0}{a_0} + \frac{r^2 + ra_0}{a_0}\cos\omega t. \tag{9}$$

Figure 3 shows a design drawing of the experimental installations and Figure 4 shows photographs of the experimental testing system. The experimental device consists of a servo motor, horizontal shaking table with fixed steel frame, belt pulley groups, and extension spring. The spring connection between the shaking table and the steel frame not only compensates for the lack of stiffness of the shaking table but also converts the table, which originally supplied the vibration environment, into one of the measured objects. When the springs are under tension, the horizontal shaking table shows a reciprocating motion with larger amplitude. The stiffness of the shaking table can be adjusted by simply replacing the springs with those of different stiffness. This experimental device has two loading modes: force and displacement. It can apply an alternating load or a constant load whose amplitude and frequency are adjustable across a large range. A conventional motor can be used as the power supply as long as the running speed is stable. The experimental device is quite small and easy to disassemble. Moreover, the device can be refitted conveniently for different research needs with high precision.

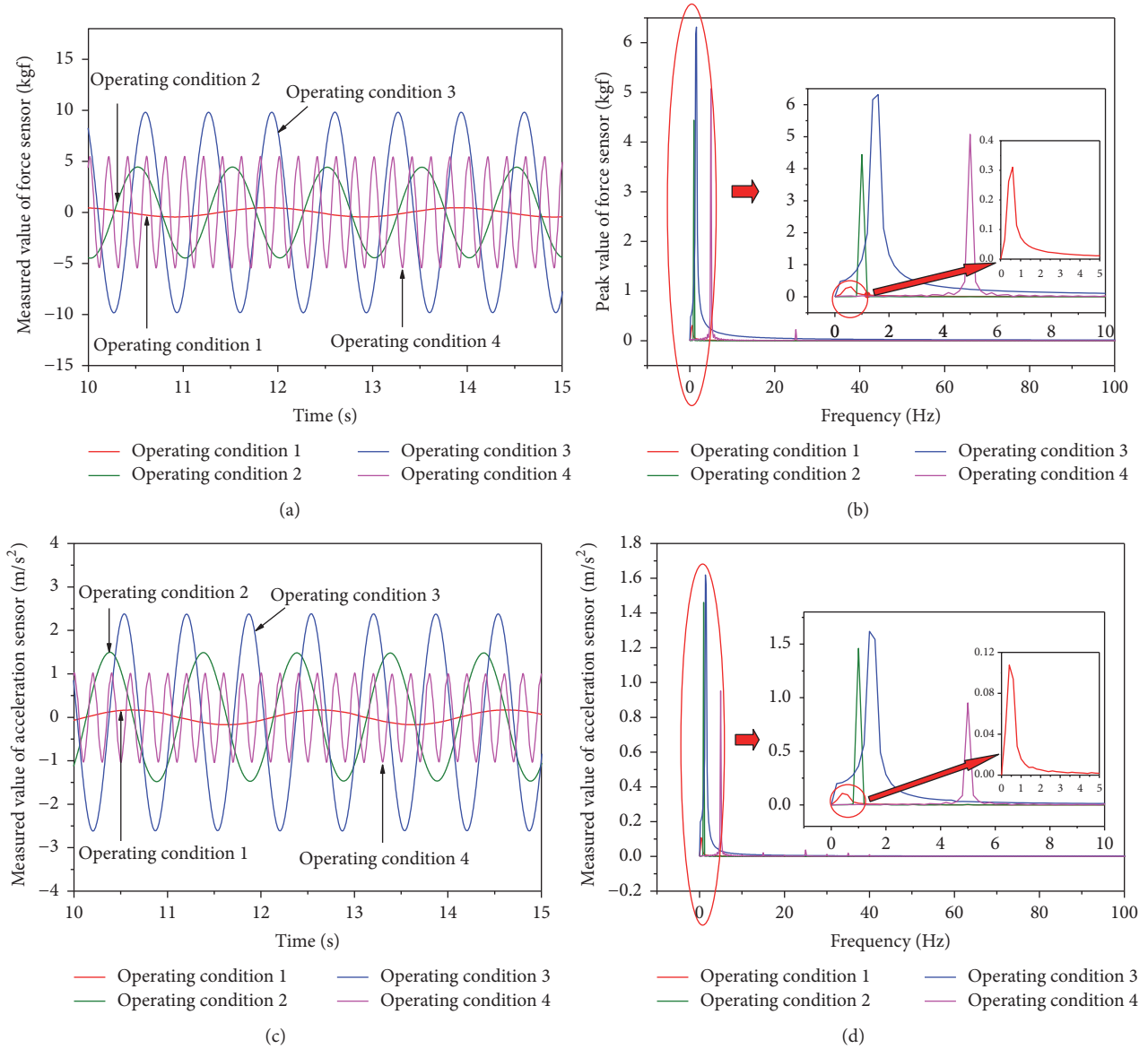

FIGURE 5: Performance test results for (a) force curve, (b) frequency spectrum of force, (c) acceleration curve, and (d) frequency spectrum of acceleration (operating condition 1: stiffness of extension spring, 100 N/m; frequency of harmonic wave, 0.5 Hz; operating condition 2: stiffness of extension spring, 460 N/m; frequency of harmonic wave, 1 Hz; operating condition 3: stiffness of extension spring, 850 N/m; frequency of harmonic wave, 1.5 Hz; operating condition 4: stiffness of extension spring, 640 N/m; frequency of harmonic wave, 5 Hz.).

The loading mode is changed by installing or removing the extension spring. The amplitude of the external load is adjusted by replacing the extension spring with one of different stiffness or by adjusting the position of the slide on the belt pulley. This is also achieved when the length of the wire rope is changed by varying the horizontal spacing or vertical height between the belt pulley and the fixed pulley. With frequency adjustment, the harmonic load signal can satisfy the frequency requirement for various experiments, ranging from low to high. The shaking table in this testing system can also be used as an experimental object. This is unlike the electromagnetic or electrohydraulic servo shaking table, which can only provide vibrations.

The results obtained from this experimental testing system are first verified. Figures 5(a)–5(d) show the force curve and acceleration curve and their corresponding frequency spectra under four operating conditions (different extension spring and total stiffness), with the frequency of the oscillatory system ranging from 0.5 to 5 Hz (sampling frequency: 204.8 Hz). The acceleration and force signals are obtained by the sensors installed on the shaking table. This shows that the high-order harmonic does not exist in the actual curve of the waveform at low frequency. In the frequency range of 0.5–5 Hz, in particular, the harmonic curve is so smooth that its accuracy satisfies the expected requirement. The waveform rapidly reaches the steady state because uncontrollable factors

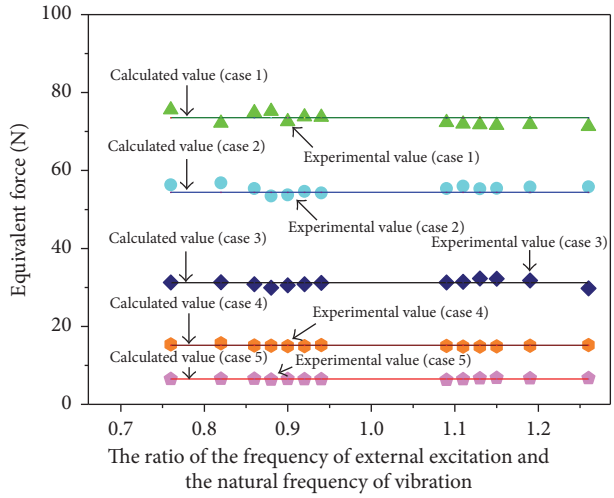

FIGURE 6: Comparison of equivalent forces with different extension springs and frequencies.

and nonlinear problems of parameters in the experimental test system have little influence on it.

Because the loading device moves with the shaking table during the operation of the vibration test system, further treatments of the experimental data are required to determine the equivalent force. Figure 6 shows a comparison between the actual equivalent force and the computed value obtained with a different loading device and extension spring. (The average equivalent force is the mean of the equivalent forces under different motor frequencies.) Under the same loading device and extension spring, the equivalent forces of the harmonic load with various frequencies are relatively constant. The maximum error of the equivalent force at a certain frequency is less than 5%; therefore, the basic experimental requirement is satisfied.

3. Analysis of TLCD Damping Characteristics

For a certain frequency band, the relevant parameters of the TLCD damping characteristics must be adjusted to achieve a good damping effect on the main structure (i.e., a smaller response and more stabilized vibration range). Owing to the characteristics of the overall and cross-sectional geometries of the TLCD, inherently nonlinear fluid damping mainly consists of head loss induced by the orifice plate, turn elbow, and, even more so, viscous damping of the shaking table. Because it is complicated to calculate each part of the damping separately, the total head loss coefficient of the TLCD is normally adopted. According to (1), the damping characteristics of the TLCD are mainly reflected in the damping force term, which is proportional to the square of the velocity and expressed as $(1/2)\rho_d A_d h_d |\dot{H}|\dot{H}$. The key parameter of the damping characteristics for a TLCD is the head loss coefficient h_d, which has been investigated in only a few studies. In published literature, the head loss coefficient was always measured and analyzed after the nonlinear damping term was transformed into the equivalent damping or linear damping term. Moreover, quantitative relationships between the head loss coefficient and other parameters of the TLCD have not yet been characterized. These problems will be studied here.

Figure 7 shows a photograph of the experimental setup. The large-amplitude loading system described in the preceding paragraph was used. Moreover, a portable digital vibrometer (PDV), which was mounted on the shaking table and fixed by a holder, could measure the axis velocity of the liquid column along the TLCD with the catopter created through light and thin floating slices or special reflective material. To analyze orifice plates of different sizes, a flange, made in the middle of the horizontal column of the TLCD, was used to change the orifice plate fixed by screws.

We assume that ρ is the liquid density; v, the axis velocity of the liquid column along the TLCD; D, the diameter of the column in TLCD; D_0, the diameter of the orifice plate; L, the total length of the liquid column; L_h, the horizontal length of the liquid column; ν, the kinematic viscosity of the liquid; and T, the period of liquid movement in the TLCD. Regardless of the variation of free surface in the liquid column and the wall effect of the column, the fluid resistance during the oscillation of liquid flow is described using these parameters:

$$F = f\left(\rho, V, D, D_0, L, L_h, \nu, T\right). \tag{10}$$

Among the nine variables in (10), ρ, V, and D are chosen as the independent variables. According to dimensional analysis, the oscillation flow force is transformed to the

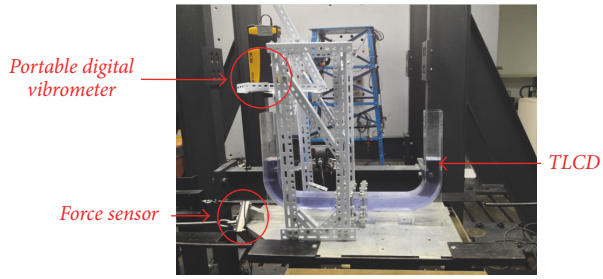

Figure 7: Testing device for TLCD.

dimensionless form $F/(\rho V^2 D^2)$. Therefore, (10) is rearranged to the following dimensionless form:

$$\frac{F}{(\rho V^2 D^2)} = f\left(\frac{D_0}{D}, \frac{L}{D}, \frac{L_h}{L_v}, \frac{\nu}{VD}, \frac{VT}{D}\right). \tag{11}$$

In (11), D_0/D represents the opening rate of the orifice plate; L/D, the shape of the vertical and horizontal liquid columns where the total length is associated with the natural period of the TLCD; and L_h/L_v, the ratio of the length between the vertical and the horizontal columns, which reflects the damping effect of the elbow in the TLCD. $\mathrm{Re} = VD/\nu$ and $K_c = VT/D$ are the Reynolds number and Keulegan–Carpenter number of the fluid, respectively.

The head loss coefficient in the TLCD is mainly determined based on the resistance part of the oscillatory flow force. The experiments are designed to identify the relationship between the head loss coefficients and other factors. The acceleration and displacement of the main structure are determined by sensors installed on the shaking table. The equivalent harmonic force of the main structure's movement is calculated by the harmonic tension measured by a force sensor. The speed of the liquid column in the TLCD is obtained by a PDV measuring the speed at the center of the liquid surface of the vertical liquid column. The experimental result for the head loss coefficient of the TLCD is obtained by using the analysis of energy method.

The shaking table with a TLCD generates a simple harmonic motion upon being driven by the motor. In a large-amplitude loading system, energy loss is inevitable; therefore, it is a nonconservative system. The total energy consumption S_{total} caused by system damping is divided into two components: the energy consumption caused by internal fluid movement of the TLCD, S_{TLCD}, and the energy consumption caused by the viscous damping of the shaking table, $S_{\text{structure}}$. The total energy consumption in one motion cycle is expressed as

$$S_{\text{total}} = \int_0^T F\dot{x}\,dt. \tag{12}$$

Here, F is the equivalent harmonic force; in addition, $\dot{x}$ is the speed of the vibration table, obtained by integrating acceleration against time. The damping energy consumption caused by the viscous damping of the shaking table is expressed as

$$S_{\text{structure}} = \int_0^T C\dot{x}\cdot\dot{x}\,dt, \tag{13}$$

where $C = 2m_s\omega_s\xi$ is the total quality and ξ is the viscous damping ratio of the shaking table. The viscous damping ratio has been obtained by experimental measurement using the free vibration attenuation method. The damping value of the hydraulic shaking table is low, so the viscous damping ratio can be calculated as $\xi = \ln(v_n/v_{n+m})/2\pi m_s$, where v_n is the displacement amplitude and v_{n+m} is the displacement amplitude after m period of motion. With the calculation of experimental data, the viscous damping ratio of this shaking table system is 0.046 (parameters for testing system: m_s = 76 kg; k_s = 1180 N/m). In one movement cycle, the energy consumption caused by the TLCD is expressed as

$$S_{\text{TLCD}} = \int_0^T \frac{1}{2}\rho A_d h_d \left|\dot{H}\right| \dot{H}\cdot\dot{H}\,dt, \tag{14}$$

where ρ is the liquid density; A_d, the cross section of the liquid column; and $\dot{H}$, the axial velocity of the liquid column surface. The basic principles of energy consumption are given as

$$\int_0^T F\dot{x}\,dt = \int_0^T C\dot{x}\cdot\dot{x}\,dt + \int_0^T \frac{1}{2}\rho A_d h_d \left|\dot{H}\right| \dot{H}\cdot\dot{H}\,dt. \tag{15}$$

Therefore, the head loss coefficient is expressed as

$$h_d = \frac{\int_0^T F\dot{x}\,dt - \int_0^T C\dot{x}\cdot\dot{x}\,dt}{\int_0^T (1/2)\,\rho A_d \left|\dot{H}\right| \dot{H}\cdot\dot{H}\,dt}. \tag{16}$$

The head loss coefficient is thus calculated by (16). Many parameters can be directly measured using the experimental instruments. The speed of the vibration table is obtained by integrating the acceleration. The structural damping ratio of the shaking table is measured by attenuating the free vibrations. The experimental data are analyzed based on the regression equation. (Data acquisition instruments are manufactured by the China Orient Institute of Noise and Vibration.)

Table 1: Experimental scheme and measured data.

Experiment number	Total length of liquid column x_1	Opening ratio x_2	Reynolds number x_3	Kc number x_4	Length of horizontal liquid column x_5	Velocity of vertical liquid column V (mm/s)	Motor speed (r/min)	Head loss coefficient
N1	19.5	0.6	9615.38	8.5	13.67	238.37	32	6.7
N2	19	0.7	10538.5	7.9	13.67	241.88	32.4	4.73
N3	20	0.5	10307.7	6.7	12.33	279.87	52.3	28.53
N4	18	0.5	9615.38	7.3	13.00	261.07	44.82	25
N5	18	0.6	10076.9	7.9	12.33	249.81	36.18	8.6
N6	18	0.4	10538.5	6.1	11.67	320.09	73.56	40.8
N7	19	0.3	10076.9	6.7	13.00	353.10	85.23	73.9
N8	17.5	0.8	10538.5	5.5	12.33	226.22	40.75	2.86
N9	19	0.4	9846.15	7.9	11.67	299.07	53.07	42.5
N10	20	0.4	10538.5	7.9	13.00	320.09	56.8	40.07
N11	18	0.6	10769.2	6.7	13.67	266.97	45.59	7.57
N12	18.5	0.4	9846.15	5.5	13.67	299.07	76.23	37.75
N13	18.5	0.8	9615.38	6.7	11.67	206.41	30.52	3.14
N14	20	0.8	10076.9	6.1	13.67	216.31	35.13	3.83
N15	19.5	0.7	10769.2	7.3	11.67	247.18	35.87	5.07
N16	18.5	0.3	10769.2	8.5	12.33	377.36	71.79	73.2
N17	20	0.7	9846.15	7.3	12.33	225.99	32.8	5.87
N18	17.5	0.3	10307.7	7.3	13.67	361.19	80.02	62.1
N19	19.5	0.5	10769.2	5.5	13.00	292.40	66.62	28.7
N20	17.5	0.7	9846.15	6.1	13.00	225.99	39.24	4.95
N21	19	0.6	10307.7	5.5	11.67	255.53	53.16	6.07
N22	17.5	0.5	10076.9	8.5	11.67	273.60	40.34	22.3
N23	17.5	0.8	9615.38	5.5	11.67	206.40	31.36	2.2

Diameter of circular orifice	Opening ratio of orifice = 0.3	Opening ratio of orifice = 0.4	Opening ratio of orifice = 0.5	Opening ratio of orifice = 0.6	Opening ratio of orifice = 0.7	Opening ratio of orifice = 0.8
	37.1 mm	37.1 mm	47.88 mm	52.44 mm	56.64 mm	60.56 mm

TLCD model	Original total length	Original horizontal length	Side length of cross section
	140 cm	60 cm	6 cm

To investigate the relationship between the oscillating force and the dimensionless terms, a series of experiments needs to be carefully designed. Uniform design [44, 45] refers to a method of experimental design that considers the distribution of test points to be even within the scope of the test. By using this method, the number of multifactor experiments can be reduced by simply recording a data sheet. The regression analysis of experimental data (e.g., quadratic polynomial regression analysis) could then be applied. The final optimal design scheme of the TLCD will be determined by discussing the influence of various factors on the experimental model.

Table 1 shows an experimental scheme according to the basic principle of uniform design. The head loss coefficients are treated as indices in the regression analysis. After obtaining the experimental result, all parameters of the factors should be normalized within their own value range. The regression equation obtained from a quadratic polynomial stepwise regression analysis is expressed as follows:

$$\begin{aligned} Y = {} & 1.761 - 9.82x_1 - 35.804x_2 - 33.475x_3 \\ & + 13.190x_4 + 26.140x_5 + 28.156x_1^2 + 127.908x_2^2 \\ & + 32.940x_3^2 + 12.713x_4^2 - 14.683x_5^2 \\ & + 26.691x_1x_2 - 3.183x_1x_3 - 37.106x_1x_4 \\ & - 17.688x_1x_5 - 13.278x_2x_3 - 37.871x_2x_4 \\ & - 28.436x_2x_5 + 10.349x_3x_4 + 0.388x_3x_5 \\ & + 12.901x_4x_5. \end{aligned} \tag{17}$$

Table 2: Partial correlation analysis of regression coefficient.

	Partial correlation coefficient	t-value	P value
$r(y, x_1)$	−0.873	2.534	0.0551
$r(y, x_2)$	−0.976	6.387	0.0078
$r(y, x_3)$	−0.982	7.280	0.0053
$r(y, x_4)$	0.903	2.971	0.059
$r(y, x_5)$	0.984	7.834	0.0043
$r(y, {x_1}^2)$	0.967	5.336	0.0129
$r(y, {x_2}^2)$	0.997	19.749	0.0003
$r(y, {x_3}^2)$	0.981	7.156	0.0056
$r(y, {x_4}^2)$	0.903	2.964	0.0593
$r(y, {x_5}^2)$	−0.953	4.421	0.0215
$r(y, x_1x_2)$	0.955	4.548	0.0199
$r(y, x_1x_3)$	−0.535	0.895	0.4367
$r(y, x_1x_4)$	−0.977	6.427	0.0076
$r(y, x_1x_5)$	−0.951	4.337	0.0226
$r(y, x_2x_3)$	−0.926	3.470	0.0403
$r(y, x_2x_4)$	−0.976	6.344	0.0079
$r(y, x_2x_5)$	−0.983	7.521	0.0049
$r(y, x_3x_4)$	0.907	3.050	0.0554
$r(y, x_3x_5)$	0.107	0.1528	0.8882
$r(y, x_4x_5)$	0.951	4.357	0.0223

Based on quadratic polynomial regression analysis, the following parameter values are obtained: F-value of regression analysis, 535.12; significance level, $P = 0.019$; Durbin-Watson statistic, 2.28551390; correlation coefficient after adjustment, $R_a = 0.9998$. Because all statistical indices meet the basic requirements for establishing the regression analysis model, the quadratic polynomial regression equation can be applied. By using the partial correlation analysis of the regression coefficient, the correlations thus obtained are tabulated in Table 2. The P values for x_1x_3 and x_3x_5 are much higher than 0.05; this indicates that neither should be included in the subsequent analysis. In other words, the interaction between the total length of the liquid column and the Reynolds number and that between the horizontal length of the liquid column and the Reynolds number have very little effect on the head loss coefficient. As shown in Table 2, single factors such as the opening rate ($x_2, {x_2}^2$), Reynolds number ($x_3, {x_3}^2$), and horizontal length of liquid column (x_5) and certain interactions such as those between the length of liquid column and the Kc number (x_1x_4), the opening rate and the Kc number (x_2x_4), and the opening rate and the horizontal length of liquid column (x_2x_5) significantly influence the head loss coefficient.

To determine the reliability of (17), five sets of experimental parameters with different combinations were randomly selected. Table 3 shows the corresponding head loss coefficients obtained in the quadratic polynomial regression equation. The head loss coefficients calculated by the regression equation are in good agreement with those obtained from the experimental results. Therefore, the quadratic polynomial regression equation can be used as the prediction equation within the scope of the experimental parameters.

To analyze the influence of various factors on the TLCD head loss coefficient more precisely, the interactions among these factors should also be considered in addition to the main effects of individual factors. By using the prediction equation within the scope of experimental parameters, parameter combinations for the head loss coefficient (e.g., Kc number–total length of liquid column–horizontal length of liquid column, opening rate–Reynolds number–Kc number, and total length of liquid column–opening rate–horizontal length of liquid column) are shown as a set of curved surfaces in Figures 8–10. For convenience of analysis, three groups of curves that reflect the impact of any two factors on the head loss coefficient are obtained by keeping another factor constant. According to the partial correlation analysis of the regression equation, terms whose P values are much higher than 0.05, such as x_1x_3 (interaction of opening rate and Reynolds number) and x_3x_5 (interaction of Reynolds number and horizontal length of liquid column), are not considered in the following analysis.

Figure 8 shows the head loss coefficient as a function of the Kc number, total length of liquid column, and horizontal length of liquid column, with other damper parameters kept constant ($x_2 = 0.5$ and $x_3 = 10191.9$). Figure 8(a) shows a three-dimensional plot of the head loss coefficient as a function of the total length of liquid column and Kc number at $x_5 =$ 11.67–13.67. Figure 8(b) shows the head loss coefficient as a function of Kc number and total length of liquid column at $x_5 = 12.67$. Figure 8(c) shows the influence of Kc number and horizontal length of liquid column on the head loss coefficient at $x_1 = 18.75$. Figure 8(d) shows the head loss coefficient as a function of the total length of liquid column for different horizontal lengths of liquid column at $x_4 = 7.0$. Figure 8(b) shows that the head loss coefficient ranges from 14.55 to 38.7 under the combined effect of both Kc number and total length of liquid column. As shown in Figure 8(c), under the interaction of the Kc number and the horizontal length of liquid column, the head loss coefficient varies from 7.0 to 23.2. In Figure 8(d), the head loss coefficient varies from 7.1 to 29.1 under the combined action of total and horizontal lengths of the liquid column. Therefore, the combined effect of Kc number and total length of the liquid column has the largest influence on the head loss coefficient.

Figure 8(b) shows that the head loss coefficient varies with different Kc numbers and total lengths of liquid column. When the total length of the liquid column is less than 17.5, the curve increases monotonically with the Kc number. Between 17.5 and 19.5, the functions are parabolic curves whose rising limb lengthens and falling limb shortens as Kc increases. Above 19.5, the head loss coefficient decreases monotonically with the Kc number. Among all monotonically decreasing curves, the spacing between curves and the gradient of the curve gradually increase with the total length of liquid column. In contrast, for monotonically decreasing curves, the gradient of the curve gradually decreases with the total length of liquid column.

Figure 8(c) shows that the vertex of the parabola shifts toward lower Kc numbers. As the horizontal length of liquid

Table 3: Comparison of head loss coefficients calculated by regression equation and experimental results.

x_1 (mm)	x_2	x_3	x_4	x_5	Experimental head loss coefficient	Numerically calculated head loss coefficient	Error
113	0.3	9615.3	8.3	74	82.61	79.91	3.27%
120	0.5	9846.2	7.0	74	21.33	22.3	4.69%
118	0.4	10384.6	6.5	78	45.72	47.96	4.90%
116	0.6	10000.0	7.9	70	9.50	9.97	4.71%
125	0.3	10538.5	7.5	70	86.59	89.9	3.82%

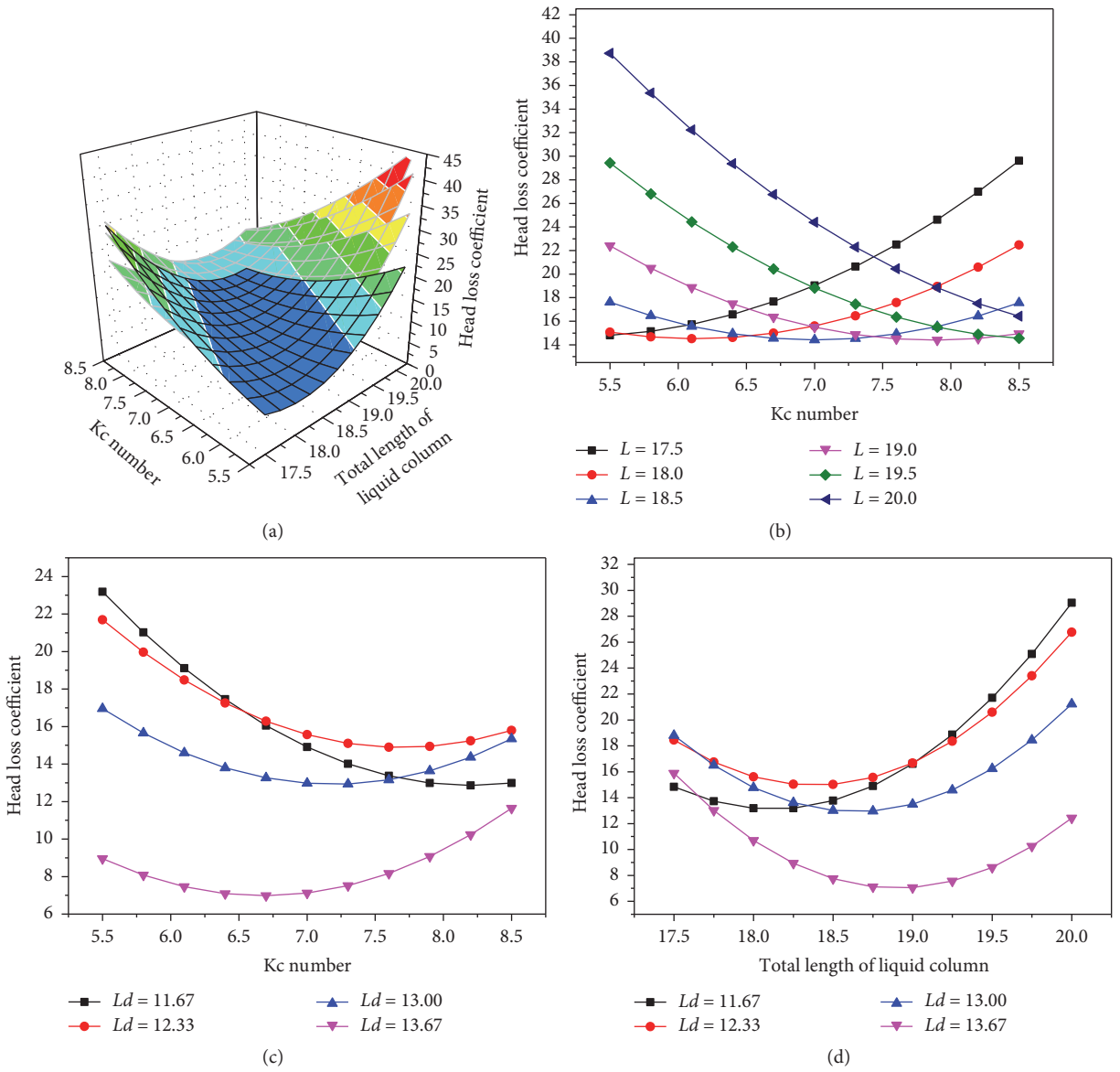

Figure 8: Relation schema of Kc number–total length of liquid column–horizontal length of liquid column.

column increases, the falling limb shortens and its gradient decreases, whereas the rising limb lengthens and its gradient increases. When the horizontal liquid column exceeds 13, the change in gradient is not apparent.

In Figure 8(d), the total length of liquid column at the vertex of the head loss coefficient parabola increases with the horizontal liquid column. In addition, the gradient of the descending part of the parabola decreases, whereas that of ascending part of the parabola increases. A comparison of Figures 8(c) and 8(d) shows that the head loss coefficients are low when the horizontal length of the liquid column reaches 13.67, regardless of the effect of the Kc number or total length of liquid column.

In general, the combined effect of the Kc number and total length of liquid column has large effects on the head loss coefficient. Because the partial correlation analysis described

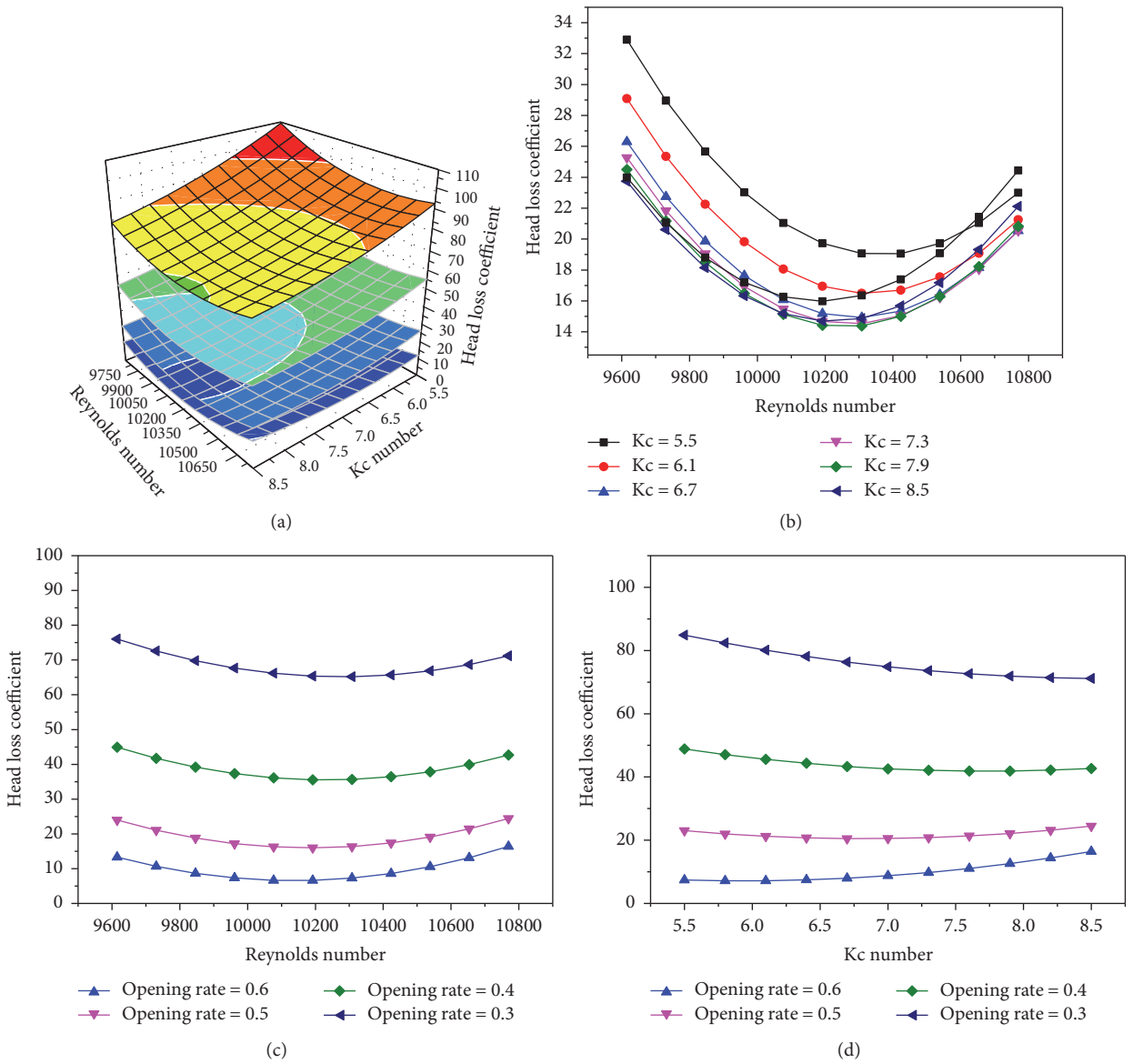

FIGURE 9: Relation schema of opening rate–Reynolds number–Kc number.

above shows that the direct influence of the other two factors is very small, the interaction has large effects on the head loss coefficient.

Figure 9 shows the head loss coefficient as a function of the opening rate, Reynolds number, and Kc number, with other damper parameters kept constant ($x_1 = 18.75$ and $x_5 = 12.67$). Figure 9(a) shows a three-dimensional plot of the head loss coefficient as a function of the Reynolds number and Kc number at $x_2 = 0.3$, 0.4, 0.5, and 0.6. Figure 9(b) shows the head loss coefficient for different Reynolds numbers and Kc numbers at $x_2 = 0.6$. Figure 9(c) shows the influence of the opening rate and Reynolds number on the head loss coefficient with $x_4 = 8.5$. Figure 9(d) shows the head loss coefficient as a function of the Kc number for different opening rates at $x_3 = 10191$.

As shown in Figure 9(b), when the Kc number increases, the vertex of the curve approaches low Reynolds numbers. In the range of 5.5 to 6.7, the gradients of the curves are similar. In contrast, when the Kc number exceeds 7.3, the gradient of the rising limb increases whereas that of the falling limb decreases.

As shown in Figure 9(c), the spacing between curves decreases with the opening rate, whereas the curvature and vertex of the curve are almost identical. With regard to the analysis shown in Figure 9(b), the curve for Kc = 8.5 in Figure 9(b) is the same as that for opening rate = 0.5 in Figure 9(c). When the Kc number changes from 8.5 to 5.5 in Figure 9(b), the head loss coefficient increases by 37% from 24.0 to 32.9 at the point of Re = 9615. When the opening rate decreases from 0.5 to 0.4 in Figure 9(c), the head loss

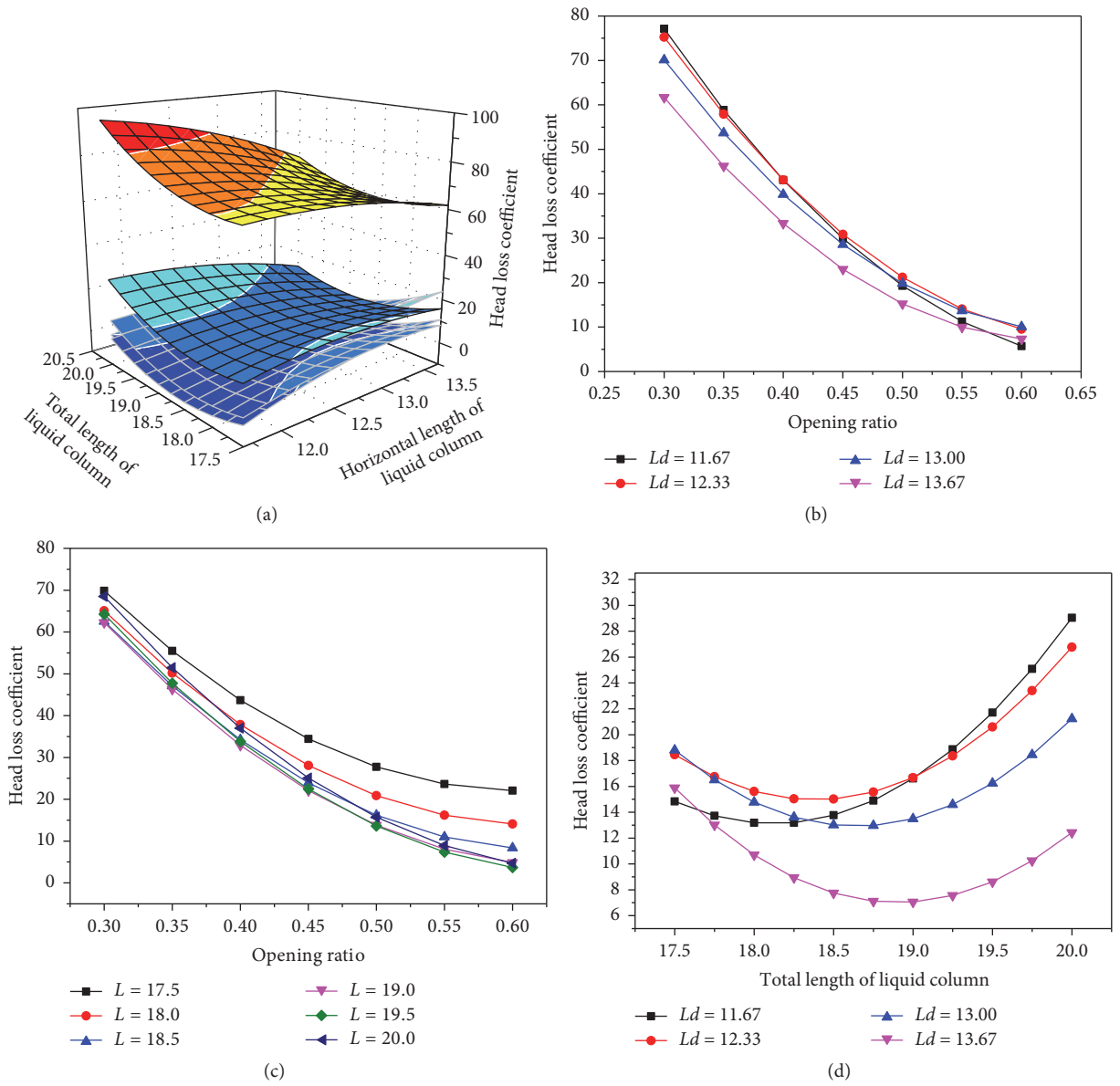

Figure 10: Relation schema of total length of liquid column–opening rate–horizontal length of liquid column.

coefficient increases by 87% from 24.0 to 44.9 at the same point. This comparison shows that even when the rate of increase for the Kc number becomes maximal (i.e., 8.5 − 5.5 = 3), the effect of the Kc number is still less than that of the opening rate (rate of increase = 0.5 − 0.4 = 0.1) on the head loss coefficient. Therefore, the head loss coefficient is more sensitive to the opening rate.

The curve spacing in Figure 9(d) changes similarly to that in Figure 9(c). In addition, the falling limb of the curve shortens and the rising limb lengthens as the opening rate increases. A comparison of Figures 9(c) and 9(d) shows that, within the experimental range of the Reynolds number, the curve spacing in Figure 9(c) remains almost unchanged, whereas that in Figure 9(d) decreases as the Kc number increases. In other words, the gradient change of the head loss coefficient as a function of the Reynolds number is greater than that as a function of the Kc number.

Figure 9 therefore shows that the opening rate has a much larger effect than other factors on the head loss coefficient. Among all two-factor combinations shown in Figure 9, the combined effect of the Kc number and the opening ratio is relatively large. However, the simple effect of the opening ratio is such that the combination effect could not alter the monotonically increasing trend of the head loss coefficient as a function of the opening ratio.

Figure 10 shows the relationship of the head loss coefficient plotted against the total length of liquid column, opening ratio, and horizontal length of liquid column, with other damper parameters kept constant (x_3 = 10537 and x_4 = 7.9). Figure 10(a) shows a three-dimensional plot of the

head loss coefficient as a function of the total length of liquid column and horizontal length of liquid column at $x_2 = 0.3$, 0.4, 0.5, and 0.6. Figure 10(b) shows the head loss coefficient as a function of the opening ratio and horizontal length of liquid column at $x_1 = 109.5$ cm. Figure 10(c) shows the influence of the total length of liquid column and opening ratio on the head loss coefficient at $x_5 = 79.6$ cm. Figure 10(d) shows the head loss coefficient as a function of the total length of liquid column for different horizontal lengths of liquid column at $x_4 = 7.0$ (discussed in the preceding paragraph). Figure 10(b) shows that the curves with different lengths of horizontal liquid column all monotonically decrease, with a gradient that continuously decreases as the opening ratio increases. Moreover, at the same opening ratio, the gradient of the curve decreases with the length of the horizontal liquid column. Similar to Figure 10(b), the gradient of the curve shown in Figure 10(c) also decreases as the opening ratio increases, but at a quicker rate. A comparison of Figures 10(b) and 10(c) shows that when the opening ratio is small, the combined effect of the opening ratio and horizontal length of liquid column has a dominant influence on the head loss coefficient. In contrast, when the opening ratio is large, the combined effect of the opening ratio and total length of liquid column dominates. Furthermore, the curve spacing in Figure 10(c) decreases as the opening ratio increases.

Figures 8–10 suggest that the main effect of the opening ratio is larger than that of the remaining two factors. When the opening ratio is large, the combined effect of the open ratio and total length of liquid column becomes dominant on the head loss coefficient. When the opening ratio is small, the combined effect of the open ratio and horizontal length of liquid column has a greater influence.

In conclusion, the opening ratio has the largest single impact on the head loss coefficient compared with other factors such as the total length of liquid column, Reynolds number, Kc number, and horizontal length of liquid column. In addition, the main effects of the Reynolds number and horizontal length of liquid column have the next largest impact, whereas the individual effects of the total length of liquid column and Kc number are the weakest. However, the combined effects among all factors also influence the head loss coefficient. The combined effect of the total length of liquid column and Kc number and that of the opening ratio and Kc number greatly influence the head loss coefficient, especially the first combination. During experiments, the head loss coefficient monotonically decreases as the opening ratio increases, regardless of the influence of the other factor.

4. Verification of Mitigation Performance under Seismic Loads and Rapid Design Strategy for TLCD Head Loss Coefficient

The motions of structures under stochastic loads need to be suppressed in practical engineering. The performance of the test system used in previous section, which is equipped with a TLCD with different head loss coefficient, is verified by numerically analyzing the structure-TLCD system under a set of recorded earthquake ground motions. As shown in Figure 11, El-Centro earthquake record (1940) is applied as an input excitation signal with Peak Ground Acceleration (PGA) 0.348 g, the first dominant frequency is 1.1 Hz, and almost three thousand time intervals among the dynamic responses under this specific excitation are employed to train the data. The parameters for testing system are the same as these in Section 3. The mass ratio between the structure and a TLCD is 5%. Figure 12(a) shows the time history responses of the test structure are controlled by the TLCD. The vibration amplitudes obtained from Fast Fourier Transform (FFT) are shown in Figure 12(b). The structural displacements have been largely reduced by the TLCD in Figure 12. A TLCD with smaller value of head loss coefficient has higher mitigation effect than that with the big one. The value of the head loss coefficient has a great influence on the mitigation effect. It is confirmed that the TLCDs used in practical engineering need to choose an optimal head loss coefficient. So the rapid design strategy for the TLCD head loss coefficient must be proposed.

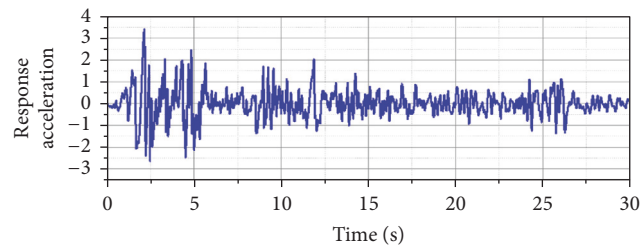

Figure 11: El-Centro earthquake record.

In order to propose the rapid design strategy for the TLCD head loss coefficient also adapting to structures under seismic loads, some key parameters should be further analyzed. Figure 13 shows the relation schema of displacement ratio between controlled structure and uncontrolled structure with different L_N/L_d and B_d/L_d. For these comparative analyses, the head loss coefficient is invariable, 2.5. L_N is the total length of a test TLCD. The displacement ratio is the ratio between the standard deviation of uncontrolled structures and the standard deviation of controlled structures. The displacement ratio reduced with the rising of the L_N/L_d, when the value of L_N is smaller than that of L_d, as shown in Figure 13(a). The rule is on the contrary for the bigger value of L_N. It is unworthy to change the total length of liquid column far from the one corresponding to the main frequency. For the evaluation of the horizontal length of liquid column, it is better to adopt a larger value, as shown in Figure 13(b). The relationship of each key parameter for test structures under seismic loads is also consistent with the relation schema in Section 4.

In real engineering projects, the head loss coefficient should be adjusted frequently to suppress the motion of the main structure more effectively. Because the head loss coefficient is affected by the total length of liquid column, opening ratio, Reynolds number, Kc number, and horizontal length of liquid column, the large number of combinations among

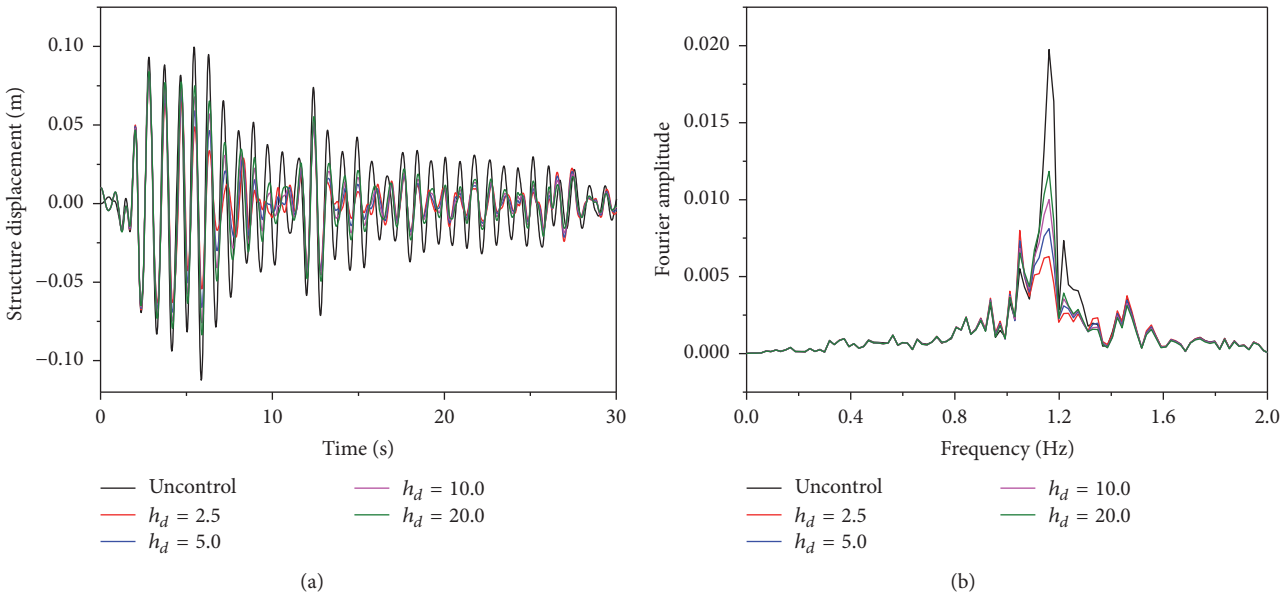

FIGURE 12: Comparison of mitigation effects with different head loss coefficient for (a) time histories of the structure displacement and (b) Fourier amplitude of the structure response.

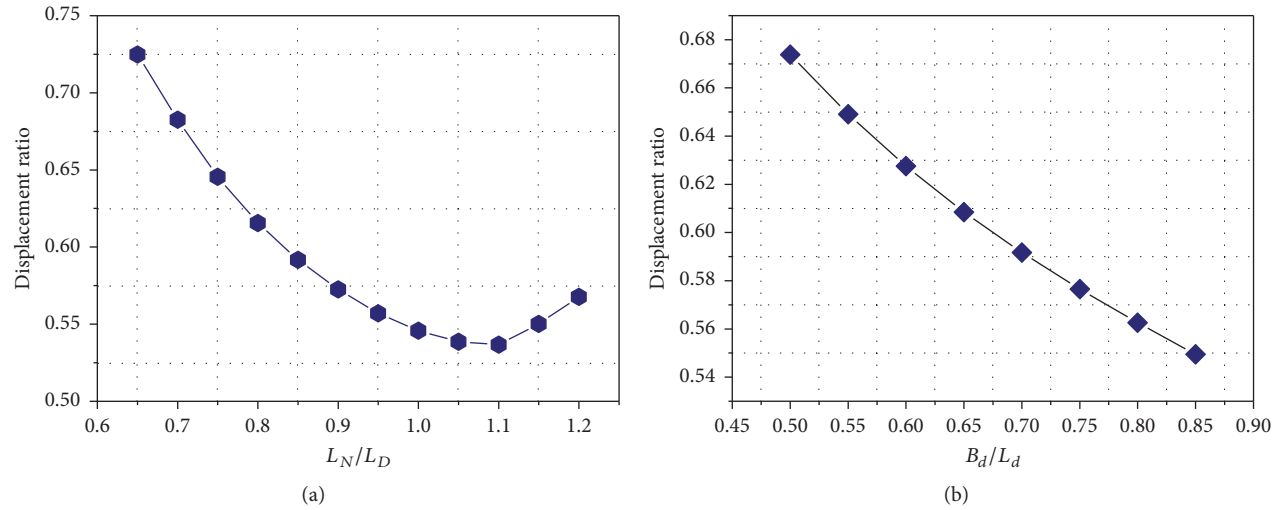

FIGURE 13: Relation schema of displacement ratio between controlled structure and uncontrolled structure.

these factors makes it difficult and inefficient to adjust them one by one. Therefore, guidelines are required for quickly adjusting the head loss coefficient to the specified value under working conditions. Here, we propose a rapid design strategy for the TLCD that is devised based on both prediction equations and variation trends in the head loss coefficient. This strategy is suitable for suppressing structures motions with low frequency and large amplitude.

In order to obtain the required head loss coefficient, every change rate of 0.1 for the opening ratio should be treated as a unit change in the head loss coefficient. Regardless of the value of other factors, the head loss coefficient will fall into the corresponding interval. Therefore, the requirement of the opening ratio should be ensured from the outset. Subsequently, according to the importance of each factor, the Reynolds number or the horizontal length of liquid column could be adjusted. Because the influence of the total length of liquid column and Kc number is mainly due to their combined effect instead of the action of each alone, adjusting these two factors accurately is extremely difficult. If the head loss coefficient reaches the required value by adjusting the opening ratio, Reynolds number, and horizontal length of liquid column, the adjustment of the total length of liquid column and Kc number is not required.

5. Conclusions

A TLCD shows promise for applications to the motion suppression of floating platforms. In this study, a specific vibration test system on land was developed to satisfy the

requirements of offshore float platforms with low frequency and large amplitude. The damping characteristic of the TLCD governs the ability of vibration suppression. The influence of various factors on the head loss coefficient was investigated for motions of the main structure with low frequency and large amplitude. The following conclusions were drawn:

(1) A vibration test system with large-amplitude motion simulation, low-frequency performance, and large stroke force (displacement) control was designed and built with simple operations and at low cost. This experimental system provided good waveforms for simple harmonic wave forces. The distortion within the low-frequency range of 0.5–1.5 Hz was less than 0.5%. The computed equivalent harmonic force showed good agreement with that obtained from experiment results with less than 5% error.

(2) In published studies, the nonlinear damping term, but not the original term, has been analyzed with linearization. In this study, the nonlinear damping term and its head loss coefficient of the TLCD were calculated based on the energy transfer between the TLCD and the main structure. Experimental data on the table displacement, table velocity, table acceleration, equivalent harmonic force, and axis velocity of liquid column along the TLCD were used for calculations.

(3) Based on the experimental method of uniform design, a reasonable and efficient experimental project was proposed to determine the variation trend in the head loss coefficient of the TLCD as a function of relevant parameters such as the total length of liquid column, opening ratio, Kc number, and Reynolds number. The prediction equation was obtained based on all the factors mentioned, whose reliability was verified from the results of random experimental tests.

(4) Variation trends in the head loss coefficient as a function of the relevant parameters were obtained in accordance with the analysis of the prediction equation. For single-factor influences on the head loss coefficient, the opening ratio of the orifice dominated, whereas the Reynolds number and horizontal length of liquid column showed the next strongest impacts. Although the total length of liquid column and Kc number showed the weakest single-factor effects on the head loss coefficient, the combined effect of these two factors was apparent. In addition, the combined effect of the opening ratio and Kc number was also prominent.

(5) A rapid design strategy for the TLCD head loss coefficient was proposed based on the changes in the head loss coefficient along with changes in TLCD-related parameters. This strategy proved highly convenient and effective for quickly adjusting the head loss coefficient to a specified value for effective vibration suppression.

Conflicts of Interest

The authors declare that they have no conflicts of interest.

Acknowledgments

The authors would like to express their gratitude for the financial support of the National Natural Science Foundation of China for Youth (Grant no. 5160916) and the State Key Laboratory Foundation of Shanghai Jiao Tong University (Grant no. 1502).

References

[1] L.-L. Zhang, J. Li, and Y. Peng, "Dynamic response and reliability analysis of tall buildings subject to wind loading," *Journal of Wind Engineering & Industrial Aerodynamics*, vol. 96, no. 1, pp. 25–40, 2008.

[2] X.-H. Zeng, X.-W. Li, Y. Liu, and Y.-X. Wu, "Nonlinear dynamic responses of tension leg platform with slack-taut tether," *China Ocean Engineering*, vol. 23, no. 1, pp. 37–48, 2009.

[3] X.-H. Zeng, X.-P. Shen, and Y.-X. Wu, "Governing equations and numerical solutions of tension leg platform with finite amplitude motion," *Applied Mathematics and Mechanics-English Edition*, vol. 28, no. 1, pp. 37–49, 2007.

[4] F. Sakai, S. Takaeda, and T. Tamaki, "Tuned liquid column damper—new type device for suppression of building vibration," in *Proceedings of International Conference on High-rise Buildings*, pp. 926–931, 1989.

[5] M. J. Hochrainer, "Tuned liquid column damper for structural control," *Acta Mechanica*, vol. 175, no. 1-4, pp. 57–76, 2005.

[6] P. A. Hitchcock, K. C. S. Kwok, R. D. Watkins, and B. Samali, "Characteristics of liquid column vibration absorbers (LCVA) - I," *Engineering Structures*, vol. 19, no. 2, pp. 126–134, 1997.

[7] P. A. Hitchcock, K. C. S. Kwok, R. D. Watkins, and B. Samali, "Characteristics of liquid column vibration absorbers (LCVA)-I,II," *Engineering Structures*, vol. 19, no. 2, pp. 135–144, 1997.

[8] H. Gao, K. S. C. Kwok, and B. Samali, "Characteristics of multiple tuned liquid column dampers in suppressing structural vibration," *Engineering Structures*, vol. 21, no. 4, pp. 316–331, 1999.

[9] S.-K. Lee, E. C. Park, K.-W. Min, S.-H. Lee, and J.-H. Park, "Experimental implementation of a building structure with a tuned liquid column damper based on the real-time hybrid testing method," *Journal of Mechanical Science and Technology*, vol. 21, no. 6, pp. 885–890, 2007.

[10] S.-K. Lee, K.-W. Min, and H.-R. Lee, "Parameter identification of new bidirectional tuned liquid column and sloshing dampers," *Journal of Sound and Vibration*, vol. 330, no. 7, pp. 1312–1327, 2011.

[11] S.-K. Lee, H.-R. Lee, and K.-W. Min, "Experimental verification on nonlinear dynamic characteristic of a tuned liquid column damper subjected to various excitation amplitudes," *The Structural Design of Tall and Special Buildings*, vol. 21, no. 5, pp. 374–388, 2012.

[12] P. Chaiviriyawong, W. C. Webster, T. Pinkaew, and P. Lukkunaprasit, "Simulation of characteristics of tuned liquid column damper using a potential-flow method," *Engineering Structures*, vol. 29, no. 1, pp. 132–144, 2007.

[13] Y.-H. Chan and Y.-J. Ding, "Passive, semi-active, and active tuned-liquid-column dampers," *Structural Engineering and Mechanics*, vol. 30, no. 1, pp. 1–20, 2008.

[14] K. A. Al-Saif, K. A. Aldakkan, and M. A. Foda, "Modified liquid column damper for vibration control of structures," *International Journal of Mechanical Sciences*, vol. 53, no. 7, pp. 505–512, 2011.

[15] L. Huo and H. Li, "Torsionally coupled response control of offshore platform structures using CTLCD," in *Proceedings of the 15th International Offrshore and Polar Engineering Conference, ISOPE-2005*, pp. 296–303, June 2005.

[16] H. H. Lee, S.-H. Wong, and R.-S. Lee, "Response mitigation on the offshore floating platform system with tuned liquid column damper," *Ocean Engineering*, vol. 33, no. 8-9, pp. 1118–1142, 2006.

[17] H. H. Lee and H. H. Juang, "Experimental study on the vibration mitigation of offshore tension leg platform system with UWTLCD," *Smart Structures and Systems*, vol. 9, no. 1, pp. 71–104, 2012.

[18] Y.-H. Chen and C.-C. Chao, "Optimal damping ratio of TLCDs," *Structural Engineering and Mechanics*, vol. 9, no. 3, pp. 227–240, 2000.

[19] K. M. Shum and Y. L. Xu, "Multiple-tuned liquid column dampers for torsional vibration control of structures: Experimental investigation," *Earthquake Engineering & Structural Dynamics*, vol. 31, no. 4, pp. 977–991, 2002.

[20] K. M. Shum, "Closed form optimal solution of a tuned liquid column damper for suppressing harmonic vibration of structures," *Engineering Structures*, vol. 31, no. 1, pp. 84–92, 2009.

[21] S. Chakraborty, R. Debbarma, and G. C. Marano, "Performance of tuned liquid column dampers considering maximum liquid motion in seismic vibration control of structures," *Journal of Sound and Vibration*, vol. 331, no. 7, pp. 1519–1531, 2012.

[22] S. K. Yalla and A. Kareem, "Semiactive tuned liquid column dampers: Experimental study," *Journal of Structural Engineering*, vol. 129, no. 7, pp. 960–971, 2003.

[23] J.-C. Wu, M.-H. Shih, Y.-Y. Lin, and Y.-C. Shen, "Design guidelines for tuned liquid column damper for structures responding to wind," *Engineering Structures*, vol. 27, no. 13, pp. 1893–1905, 2005.

[24] J.-C. Wu, Y.-P. Wang, C.-L. Lee, P.-H. Liao, and Y.-H. Chen, "Wind-induced interaction of a non-uniform tuned liquid column damper and a structure in pitching motion," *Engineering Structures*, vol. 30, no. 12, pp. 3555–3565, 2008.

[25] J.-C. Wu, C.-H. Chang, and Y.-Y. Lin, "Optimal designs for non-uniform tuned liquid column dampers in horizontal motion," *Journal of Sound and Vibration*, vol. 326, no. 1-2, pp. 104–122, 2009.

[26] J.-C. Wu, Y.-P. Wang, and Y.-H. Chen, "Design tables and charts for uniform and non-uniform tuned liquid column dampers in harmonic pitching motion," *Smart Structures and Systems*, vol. 9, no. 2, pp. 165–188, 2012.

[27] T. Sarpkaya, In-line and transverse forces on smooth and sand-roughened cylinders in oscillatory flow at high reynolds numbers. Naval Postgraduate School 1976.

[28] T. Sarpkaya, "Vortex-induced oscillations," *Journal of Applied Mechanics*, vol. 46, no. 2, pp. 241–258, 1979.

[29] T. Sarpkaya and M. Isaacson, Mechanics of Wave Forces on Offshore Structures. Van Nostrand Reinhold. New York 1981.

[30] T. Sarpkaya, "Hydrodynamic damping, flow-induced oscillations, and biharmonic response," *Journal of Offshore Mechanics and Arctic Engineering*, vol. 117, no. 4, pp. 232–238, 1995.

[31] J. Carberry, Wake states of a submerged oscillating cylinder and of a cylinder beneath a free-surface. Dissertation. Monash University 2002.

[32] T. L. Morse and C. H. K. Williamson, "Employing controlled vibrations to predict fluid forces on a cylinder undergoing vortex-induced vibration," *Journal of Fluids and Structures*, vol. 22, no. 6-7, pp. 877–884, 2006.

[33] J. X. Yu and M. Y. Fu, "Fatigue reliability analysis of vortex-induced vibration of submarine pipeline span," *Journal of Tianjin University*, vol. 41, no. 11, pp. 1321–1325, 2008.

[34] J.-X. Yu, H.-L. Xu, C.-M. Yuan, and Z.-C. Wang, "Fatigue reliability analysis of vortex induced vibration of TLP tethers in waves and current," *Journal of Ship Mechanics*, vol. 12, no. 4, pp. 592–598, 2008.

[35] J.-H. Kim, J.-H. Kim, S.-H. Jeong, and B.-W. Han, "Design and experiment of an electromagnetic vibration exciter for the rapping of an electrostatic precipitator," *Journal of Magnetics*, vol. 17, no. 1, pp. 61–67, 2012.

[36] H. Li, B. Yang, G. Yan, and J. Hu, "Vibration control simulation of an electrodynamic shaker based on an electromagnetic finite element model," *International Journal of Applied Electromagnetics and Mechanics*, vol. 39, no. 1-4, pp. 769–777, 2012.

[37] D. Zhu, S. Roberts, M. J. Tudor, and S. P. Beeby, "Design and experimental characterization of a tunable vibration-based electromagnetic micro-generator," *Sensors and Actuators A: Physical*, vol. 158, no. 2, pp. 284–293, 2010.

[38] J. M. Oliver and S. Priya, "Design, fabrication, and modeling of a four-bar electromagnetic vibration power generator," *Journal of Intelligent Material Systems and Structures*, vol. 21, no. 13, pp. 1303–1316, 2010.

[39] J. P. Conte and T. L. Trombetti, "Linear dynamic modeling of a uni-axial servo-hydraulic shaking table system," *Earthquake Engineering & Structural Dynamics*, vol. 29, no. 9, pp. 1375–1404, 2000.

[40] M. Stehman and N. Nakata, "Direct acceleration feedback control of shake tables with force stabilization," *Journal of Earthquake Engineering*, vol. 17, no. 5, pp. 736–749, 2013.

[41] Y. Jianjun, J. Guilin, D. Duotao, and L. Sheng, "Acceleration harmonic identification for an electro-hydraulic servo shaking table based on the normalized least-mean-square adaptive algorithm," *Journal of Vibration and Control*, vol. 19, no. 1, pp. 47–55, 2013.

[42] Y. Dozono, T. Horiuchi, H. Katsumata, and T. Konno, "Shaking-table control by real-time compensation of the reaction force caused by a nonlinear specimen," *Journal of Pressure Vessel Technology, Transactions of the ASME*, vol. 126, no. 1, pp. 122–127, 2004.

[43] B. Ye, G. Ye, W. Ye, and F. Zhang, "A pneumatic shaking table and its application to a liquefaction test on saturated sand," *Natural Hazards*, vol. 66, no. 2, pp. 375–388, 2013.

[44] K.-T. Fang, D. K. Lin, P. Winker, and Y. Zhang, "Uniform design: theory and application," *Technometrics. A Journal of Statistics for the Physical, Chemical and En*, vol. 42, no. 3, pp. 237–248, 2000.

[45] K.-T. Fang and F. J. Hickernell, "Uniform experimental design," in *Uniform Experimental Design, in Encyclopedia on Statistics in Quality and Reliability*, vol. 4, pp. 2037–2040, Wiley, 2008.